Comparison of Complementary and Modular Linear Flux-Switching Motors With Different Mover and Stator Pole Pitch

Ruiwu Cao[1], Ming Cheng[1], Chris Mi[2], Wei Hua[1], and Wenxiang Zhao[3]

[1]School of Electrical Engineering, Southeast University, Nanjing 210096, China
[2]College of Engineering and Computer Science, University of Michigan, Dearborn, MI 485 USA
[3]School of Electrical and Information Engineering, Jiangsu University, Zhenjiang 212013, China

Linear flux-switching permanent magnet (LFSPM) motors with both permanent magnets and armature windings on the short primary mover have attracted considerable attention due to their simple and cheap stator which only consists of iron. Hence, this kind of liner motor is very suitable for long stator applications such as in urban rail transportations. However, the conventional LFSPM motors directly split from rotary FSPM motor suffer from drawbacks such as unbalanced magnetic circuit of end coil, heavy mover, and bigger cogging force and force ripple. Modular LFSPM (MLFSPM) motors can mitigate the problem of unbalanced magnetic circuit of end coil. But some MLFSPM motors with different stator/mover pole pitch $\tau_s/\tau_m = 12/14, 12/10$ don't have complementary phase armature windings, which will lead to asymmetrical and non-sinusoidal back-electromotive force, bigger cogging force and thrust force ripple. The key of this paper is to propose, investigate, and compare four complementary and modular structures for the LFSPM motors with different τ_s/τ_m. The electromagnetic performance and dimensions of the proposed complementary MLFSPM motors with different τ_s/τ_m are investigated, compared and confirmed by the means of finite element analysis and experimental results. Based on the analysis results, two complementary MLFSPM motors with $\tau_s/\tau_m = 12/13$ are chosen to be the two best motors, which can offer the biggest thrust force, relatively smaller cogging force and thrust force ripple, and shorter mover length.

***Index Terms*—Complementary and modular, flux-switching permanent magnet motor, linear motor, permanent magnet motor.**

I. INTRODUCTION

LINEAR motors produce a direct thrust force without the need of conversion from rotational torque to linear force. Therefore, they are ideal for rail transportation systems [1]–[5]. In recent years, a new kind of linear primary permanent magnet (LPPM) motor [6]–[9], namely the linear structure of stator-PM motors [10], doubly salient permanent magnet (DSPM) motors [11], flux reversal permanent magnet (FRPM) motors [12], and flux-switching permanent magnet (FSPM) motors [13], have attracted wide attention, in which both the permanent magnets and the armature windings are placed in the short primary mover, while the long secondary stator is only made of iron. Hence, this kind of LPPM motors incorporates the merits of simple structure of linear induction motors and linear switched reluctance (LSR) motors, and high power density of linear synchronous PM (LSPM) motors, which are perfectly suited for long stator applications.

It has been identified that FSPM motors can offer high power density [14], [15], sinusoidal back-electromotive force (EMF), and fault-tolerance capacities [16], [17], compared with DSPM motors.

The conventional linear FSPM (LFSPM) motors directly split from the rotary FSPM motors without additional teeth will suffer from the drawbacks of unbalanced magnetic circuit in the end coil and bigger cogging force. In order to balance the end effect for the end coil of the conventional LFSPM motors, two additional teeth are added at each end of its mover [9]. Also, the cogging force can be reduced by adjusting the additional teeth position [18]. However, these two additional teeth can't totally balance the unbalanced magnetic circuit of the end coils because the flux-linkage in the middle coils is excited by two PMs while the one of the end coils is just excited by one PM. To solve the unbalanced magnetic circuit problem, a modular LFSPM (MLFSPM) motor based on a 12/14-pole rotary FSPM motor has been proposed in [19]. So the back-EMF of middle coils, end coils, and three phase coils are balanced. Also, the magnet utilization ratio of the MLFSPM motor is higher than the conventional LFSPM motor when the volume of each PM is the same. However, this MLFSPM motor based on the 12/14-pole rotary FSPM motor suffers from the drawbacks of non-sinusoidal back-EMF especially at higher air-gap flux density, bigger cogging force and thrust force ripple due to the two coils of each phase without complementary performance. To incorporate the merits and mitigate the deficiency of this motor, a complementary MLFSPM (CMLFSPM) motor has been proposed and investigated in [20].

However, current MLFSPM and CMLFSPM motors are mainly based on the three-phase 12/14-pole rotary FSPM motor. In order to obtain an optimal CMLFSPM motor with bigger thrust force, smaller cogging force and thrust force ripple based on the same total PM volume and other key parameters, it is necessary to investigate different stator and mover pole pitch (τ_s/τ_m) structures. The key of this paper is to fully investigate and quantitatively compare different CMLFSPM motors with τ_s/τ_m = 12/10, 12/11, 12/12, 12/13, 12/14, and 12/15. Based on this analysis, some new MLFSPM motors with different τ_s/τ_m are proposed, investigated and compared. Then, the best structure and stator/mover pole pitch are obtained.

II. LFSPM MOTORS BASED ON 12/14-POLE FSPM MOTOR

The operation principle and electromagnetic performance of a $P_{\rm m}/P_{\rm s} = 12/14-$ pole FSPM motor have been investigated

Manuscript received July 15, 2012; revised November 28, 2012; accepted December 03, 2012. Date of publication December 10, 2012; date of current version March 20, 2013. Corresponding author: M. Cheng (e-mail: mcheng@seu.edu.cn).

Color versions of one or more of the figures in this paper are available online at http://ieeexplore.ieee.org.

Digital Object Identifier 10.1109/TMAG.2012.2233208

in [21], [22], where P_{m} and P_{s} are the stator and rotor pole number of a rotary FSPM motor, respectively. A conventional liner FSPM (LFSPM) motor as shown in Fig. 1(a) can be obtained by splitting the rotary 12/14-pole FSPM motor along the radial direction and unrolling it. Also, in order to balance the magnet circuit for the end coils, two additional teeth are added at each end of the primary mover, which is named as "$4*\mathrm{ABC}$" in this paper. The basic E-shaped module and some key parameters of this motor are defined as shown in Fig. 1(b). To balance the magnetic circuit for the end coils and enhance the magnet utilization, a MLFSPM motor shown in Fig. 1(c), named as "ABCABC" in this paper, has been investigated and compared with a "$4*\mathrm{ABC}$" in [19]. It can be seen from Fig. 1(c) that "ABCABC" can be obtained from "$4*\mathrm{ABC}$" by replacing its PM with flux barrier and using alternate armature windings. Also, the two PMs in the two adjacent E-shaped modules are magnetized in opposite direction. Each phase consists of two E-shaped modules whose positions are mutually λ_1 apart:

$$\lambda_1 = \left(\frac{P_m}{2}\right)\tau_m = 7\tau_s \tag{1}$$

where τ_s is the stator pole pitch, τ_m is the mover pole pitch. Also, for a three-phase motor, the relative displacement between the two E-shaped modules of adjacent two phases is

$$\lambda_2 = 2\tau_m = 2\tau_s P_s/P_m = 7\tau_s/3 = (2+1/3)\tau_s. \tag{2}$$

It can be seen from (1) and (2) that motor "ABCABC" is a three-phase motor and each phase consists of two E-shaped modules, which have the same relative position with stator. However, for the rotary FSPM motor and motor "$4*\mathrm{ABC}$", each phase consists of two sets of complementary coils, that is, coil A1+coil A3 is complementary with coil A2+coil A4. Hence, their back-EMF waveforms are sinusoidal because the even harmonics in the back-EMF of phase coils are significantly reduced. Hence, it can be predicted that the back-EMF waveform of motor "ABCABC" is not sinusoidal.

To obtain a CMLFSPM motor, two methods can be adopted in motor "ABCABC". First, the left three E-shaped modules of motor "ABCABC" move to the left about $0.5\tau_{\mathrm{s}}$, namely $\lambda_1 = 7.5\tau_s$, as shown in Fig. 1(d). Then the electromagnetic performances of the two coils of phase A are mutually 0 electrical degrees (0°) apart. Hence, the even harmonics in the back-EMF of phase A can be significantly reduced. This structure is named as "ABC-ABC" in this paper.

Second, as shown in Fig. 1(e), the two E-shaped modules of one phase can be put together whose minimum position are mutually λ_1 apart:

$$\lambda_1 = (j \pm 1/2)\tau_s. \tag{3}$$

For a three-phase motor, the relative displacement between the two E-shaped modules of the adjacent two phases must satisfy:

$$\lambda_2 = (k \pm 1/3)\tau_s \quad \text{or} \quad \lambda_2 = (k \pm 1/6)\tau_s \tag{4}$$

where j and k are positive integer (In Fig. 1(e), $j=2$, $k=5$, $\lambda_1 = 2.5\tau_s$, and $\lambda_2 = (5+1/3)\tau_{\mathrm{s}}$). This structure is named as "AABBCC" in this paper.

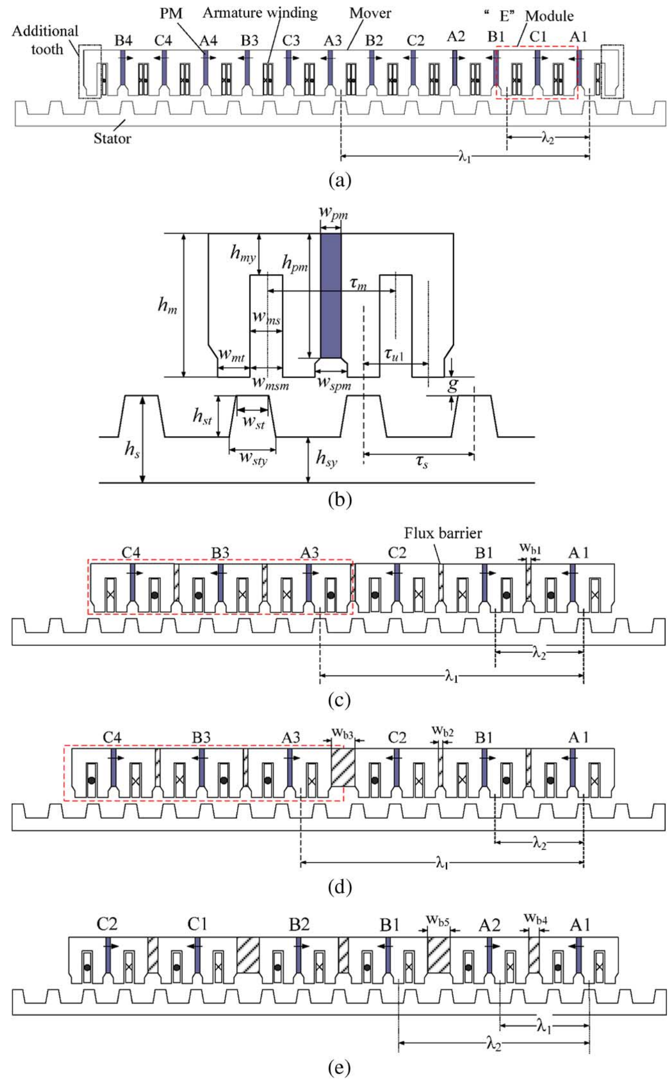

Fig. 1. The cross-section of the LFSPM motors based on 12/14-pole FSPM motors. (a) Motor "$4*\mathrm{ABC}$". (b) E-shaped module. (c) Motor "ABCABC". (d) Motor "ABC-ABC". (e) Motor "AABBCC".

A. Dimension Analysis of LFSPM Motors

To optimize, analyze, and compare different LFSPM motors, it is necessary to explain some key parameters and define some coefficients.

- Different from a rotary FSPM motor, the PMs are designed a little shorter than the mover tooth. The mover tooth width w_{mt}, the slot open width w_{ms}, and the width of the slot under PM w_{spm} as shown in Fig. 1(b) satisfy the relationship $w_{mt} = w_{ms} = w_{spm} = \tau_m/4$.
- To obtain the best structure and coefficient τ_s/τ_m, the mover height h_m, the motor stack length l_m, and air gap length g, mover yoke height h_{my}, stator tooth height h_{st}, stator yoke height h_{sy}, mover pole pitch τ_m, total PM volume, stator height h_{s}, applied peak phase current $I_{\max}$ and total phase armature winding number of all the LFSPM motors are kept constant and designed the same as an optimized prototype motor as listed in Table I. For this prototype motor, some key parameters of the mover iron, PM, and stator teeth dimension have been optimized, but

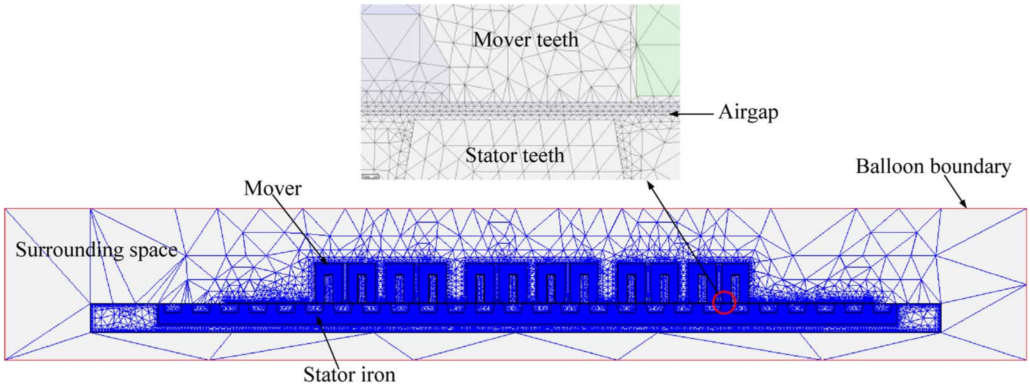

Fig. 2. Generated mesh and FEA model of the prototype motor “AABBCC” with $\tau_s/\tau_m = 12/14$.

TABLE I
DESIGN SPECIFICATIONS OF MOTOR “AABBCC” WITH $\tau_s/\tau_m = 12/14$

Items	Specifications
Rated speed, v (m/s)	1.5
Mover width, w_m (mm)	120
Mover pole pitch, τ_m (mm)	42
Stator pole pitch, τ_m (mm)	τ_m*12/14
Mover tooth width, w_{mt} (mm)	τ_m/4
Mover slot mouth width, w_{msm} (mm)	τ_m/4
Slot width (Under PM), w_{spm} (mm)	τ_m/4
Mover height, h_{my} (mm)	50
Mover yoke height, h_{my} (mm)	14
Magnet height, h_{pm} (mm)	0.9* h_m
Magnet width, w_{pm} (mm)	7
Air gap length, g (mm)	1
Stator tooth width, w_{st} (mm)	1.1*τ_m/4
Stator teeth yoke width, w_{sty} (mm)	1.5*τ_m/4
Stator tooth height, h_{st} (mm)	12
Stator yoke height, h_{sy} (mm)	15
Stator height, h_s (mm)	27
Copper filling factor, k_{slott}	0.4
Phase resistance (Ω)	1.5
Number of turns per coil, N_{coil}	116
Rated current I_{rms} (A)	6

the detailed optimization procedure will not be discussed in this paper.

- The stator tooth width and stator tooth-yoke coefficients are defined as

$$k_{st} = \frac{w_{st}}{\left(\frac{\tau_m}{4}\right)} \tag{5}$$

$$k_{sty} = \frac{w_{sty}}{\left(\frac{\tau_m}{4}\right)}. \tag{6}$$

Because coefficient k_{st} is sensitive to the cogging force and force ripple and k_{sty} affects the magnet saturation in the stator teeth, k_{st} and k_{sty} are optimized for different LFSPM motors while other parameters are kept constant as listed in Table I.

- $w_{b1} = w_{pm}$ is the flux barrier width of motor “ABCABC”, $w_{b2} = w_{b1} = w_{pm}$, and w_{b3} are the flux barrier width of motor “ABC-ABC”, w_{b4} and w_{b5} are the flux barrier width of motor “AABBCC”.
- The average thrust force and force ripple of all motors are calculated by means of FEA based on $i_d = 0$ control method, namely, the angle between back-EMF and current equal to zero. For LFSPM motors, the average thrust force reaches nearly the maximum value based on this method because its $d - q$ frame inductance L_d and L_q are nearly the same [19].

It can be seen from Fig. 1(a) that the total PM volume of the four types of motors is the same, so the width of each PM of motor “4∗ABC” is $0.5 * w_{pm}$. Hence, the mover length of motor “4 ∗ ABC” can be calculated as $L_m = 13\tau_m - 0.5 * w_{pm}$. Also, the mover length of motor “ABCABC” and “ABC-ABC” can be calculated as $L_m = 12\tau_m - w_{pm}$ and $L_m = 12\tau_m - w_{pm} + 0.5\tau_s = 14.5\tau_s - w_{pm}$, respectively.

For motor “AABBCC”, the length of one E-shaped module can be expressed as

$$w_E = 2\tau_m - w_{pm} = 2\tau_s P_s/P_m - w_{pm}. \tag{7}$$

It can be seen that w_E reaches the maximum value when $w_{pm} = 0$. Hence, the maximum value of w_E can be obtained as

$$w_E = 7\tau_s/3 < 2.5\tau_s. \tag{8}$$

So, the minimum value of $\lambda_1 = 2.5\tau_s$ is adopted for this motor.

It can be seen from Fig. 1(e) that the flux barrier width w_{b4} can be expressed as

$$w_{b4} = 2.5\tau_s + w_E = \tau_s/6 + w_{pm}. \tag{9}$$

So the total length of phase A module w_{AA} can be derived as

$$w_{AA} = 2w_E + w_{b4} = 29\tau_s/6 - w_{pm}. \tag{10}$$

It can be seen from (10) that w_{AA} reaches the maximum value when $w_{pm} = 0$. The maximum value of w_{AA} can be calculated as

$$w_{AA} = 29\tau_s/6 < 5\tau_s. \tag{11}$$

Hence, for a three-phase motor, the three shortest relative displacements between the two adjacent phase modules λ_2 of “AABBCC” motors can adopt the following values:

$$\lambda_2 = (5 \pm 1/6)\tau_s, \quad \text{or} \quad \lambda_2 = (5 + 1/3)\tau_s. \tag{12}$$

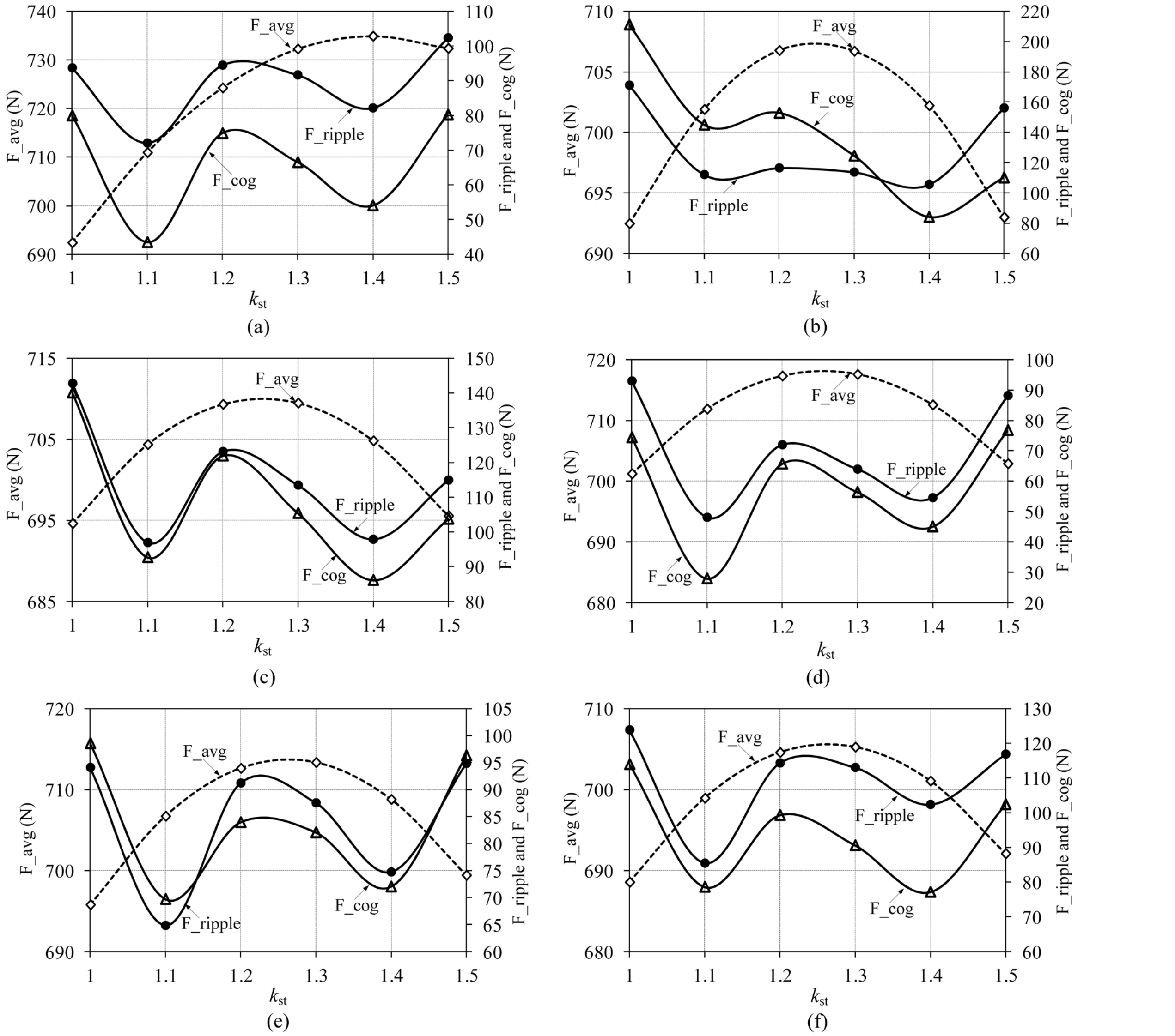

Fig. 3. Force performance of the six LFSPM motors versus different k_{st}. (a) Motor "$4*\mathrm{ABC}$", (b) Motor "ABCABC", (c) Motor "ABC-ABC", (d) Motor "AABBCC" with $\lambda_2 = (5+1/3)\tau_s$, (e) Motor "AABBCC" with $\lambda_2 = (5+1/6)\tau_s$, (f) Motor "AABBCC" with $\lambda_2 = (5-1/6)\tau_s$.

The width of the flux barrier between adjacent phase modules w_{b5} can be expressed as

$$w_{b5} = \lambda_2 - w_{AA}. \tag{13}$$

The total mover length can be expressed as

$$L_m = 3w_{AA} + 2w_{b5}. \tag{14}$$

Thus, by substituting (10), (12), and (13) into (14), the total mover length of the three shortest mover "AABBCC" motors can be calculated as

$$L_m = \begin{cases} 93\tau_m/7 - w_{pm}, & \lambda_2 = (5+1/3)\tau_s \\ 91\tau_m/7 - w_{pm}, & \lambda_2 = (5+1/6)\tau_s\,. \\ 87\tau_m/7 - w_{pm}, & \lambda_2 = (5-1/6)\tau_s \end{cases} \tag{15}$$

B. Electromagnetic Performance Comparison

As aforementioned, the dimensions of the six LFSPM motors have been discussed in Section II-A. In this section, the electromagnetic performance of the six motors will be investigated using finite element analysis (FEA). The transient solver of Ansys Maxwell-2D software is used to solve the electromagnetic characteristic of the proposed motors. Fig. 2 shows the generated mesh of FEA model, in which a balloon boundary is applied at the edge of the surrounding space of the motor. To obtain enough accurate cogging and thrust force results, the air gap is meshed by four layers. After meshing with triangle-shaped elements, a total of 116619 elements are generated.

Based on FEA, the peak to peak value of cogging force F_cog, average thrust force F_avg and thrust force ripple F_ripple at the rated current of motor "$4*\mathrm{ABC}$" for k_{st} in the range of 1 to 1.5 are calculated and shown in Fig. 3(a). It can be seen that F_cog and F_ripple reach the minimum value at $k_{st} = 1.1$, while F_avg is about 97% of the maximum value at $k_{st} = 1.4$. Hence, $k_{st} = 1.1$ is adopted in motor "$4*\mathrm{ABC}$". Similarly, as can be seen from Fig. 3(b)–(f), $k_{st} = 1.4$ is adopted in motor "ABCABC" and motor "ABC-ABC" and $k_{st} = 1.1$ is adopted in motors "AABBCC" with $\lambda_2 = (5+1/3)\tau_s$, $\lambda_2 = (5+1/6)\tau_s$, and $\lambda_2 = (5-1/6)\tau_s$, respectively.

TABLE II
COMPARISON OF THE SIX MOTORS WITH $\tau_s/\tau_m = 12/14$

Structure	4*ABC	ABCABC	ABC-ABC	AABBCC		
				λ_2=(5+1/3)τ_s	λ_2=(5+1/6)τ_s	λ_2=(5-1/6)τ_s
k_{st}	1.1	1.4	1.4	**1.1**	1.1	1.1
k_{sty}	1.5					
τ_s	$6\tau_m/7$					
EMF (V)	58.76	60.65	60.49	**61.3**	59.75	59.56
$F_{\_avg}$ (N)	710.9	702.2	704.8	**711.86**	706.71	698.94
$F_{\_cog}$ (N)	43.45	80.88	86.05	**27.89**	69.68	78.57
$F_{\_ripple}$ (N)	72	**105.47**	97.8	**48**	64.8	85.41
V_{m_iron} (cm^3)	**2375.1**	1958.04	1958.04	**1958.04**	1958.04	1958.04
V_{PM} (cm^3)	Same	Same	Same	**Same**	Same	Same
M_{copper} (kg)	Same	Same	Same	**Same**	Same	Same
L_m (mm)	$91\tau_m/7-0.5*w_{pm}$	$84\tau_m/7-w_{pm}$	$87\tau_m/7-w_{pm}$	**$93\tau_m/7-w_{pm}$**	$91\tau_m/7-w_{pm}$	$87\tau_m/7-w_{pm}$
L_m/L_{m1}(%)	**100%**	**91.6%**	95%	**101.6%**	99.4%	95%

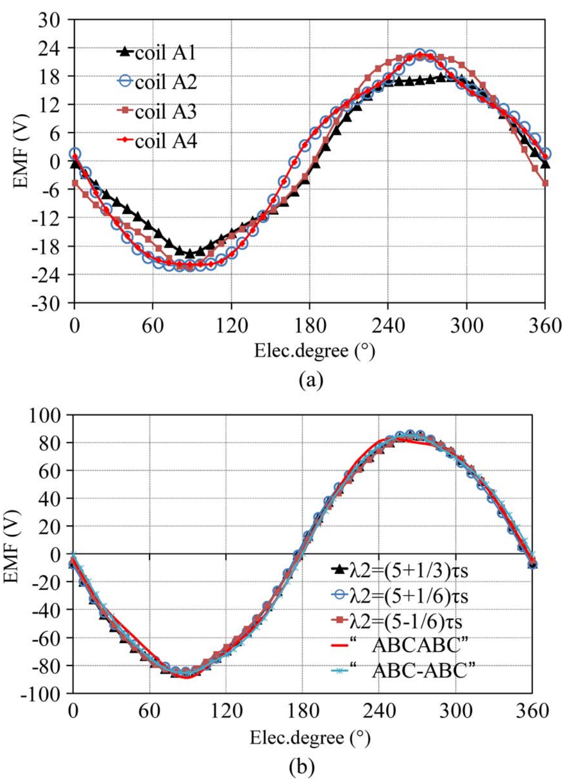

Fig. 4. Back-EMF waveforms in Phase A of the six LFSPM motors. (a) Motor "$4*$ABC". (b) Motor "ABCABC", "ABC-ABC", and "AABBCC" motors.

It can be seen from Fig. 4(a) that the back-EMF of motor "$4*$ABC" in end coil A1 is smaller than the one in coil A3, which is caused not only by the end effect but also by the asymmetrical magnetic circuit in both coils. However, the back-EMF waveforms in the middle coil A2 and coil A4 are nearly the same. Also, it can be seen from Fig. 4(b) that the negative half back-EMF of motor "ABCABC" is different from the positive half, which is caused by the non-complementary magnetic circuit in the two coils of phase A, while the back-EMF waveforms of the four complementary and modular motors, namely motor "ABC-ABC" and the three "AABBCC" motors, are symmetrical.

For comparison, the detailed electromagnetic performances of the aforementioned six motors at optimal k_{st} are listed in Table II. From Table II, the electromagnetic performances of the six motors can be summarized as:

- The thrust force generated by per unit volume of PM of the six motors is nearly the same when the same total PM volume is used.
- Because motor "ABCABC" without complementary phase coils, hence it has asymmetrical back-EMF and bigger force ripple. But it has the shortest mover length.
- Because each PM width of motor "$4*\mathrm{ABC}$" is half of the one of the other LFSPM motors, its mover iron volume is about 121% of the other LFSPM motors.
- The cogging force and force ripple of "AABBCC" motors are smaller than those of motor "ABCABC" and "ABC-ABC".
- The volume of each stator teeth of motor "ABCABC" and "ABC-ABC" is the same which is about 111.5% of other motors.
- Motor "AABBCC" with $\lambda_2 = (5+1/3)\tau_s$ can offer the biggest F_avg, the smallest F_cog and F_ripple. But it has the longest mover, which is about 101.6% of motor "$4*\mathrm{ABC}$". Hence, considering the mover length, F_avg, F_ripple, and F_cog, this motor is chosen to be the best one when $\tau_s/\tau_m = 12/14$.

To validate the associated FEA results of the LFSPM motors in Table II, a three-phase motor prototype based on the optimized dimension of motor "AABBCC" with $\lambda_2 = (5+1/3)\tau_s$ as shown in Table I has been built. The detailed structure including the mover, stator, U-shaped laminated segment, and the prototype motor are shown in Fig. 5. The simulation and measured open circuit back-EMF waveforms at speed of 1.05 m/s are compared in Fig. 6(a) and (b). Fig. 6(c) shows the FEA ($I_{\max} = 5$ A, 7 A, and 9 A) and measured ($I_{\max} = 5$ A) locked thrust force waveforms versus electrical position β. It can be seen that the thrust force reaches the maximum value around $\beta = 90°$, where the back-EMF of phase A reaches the maximum value. The applied DC currents in Phase A, Phase B, and Phase C satisfy the following relationship: $I_a = I_{\max}$, $I_b = I_c = -I_{\max}/2$. It can be seen that the simulation results

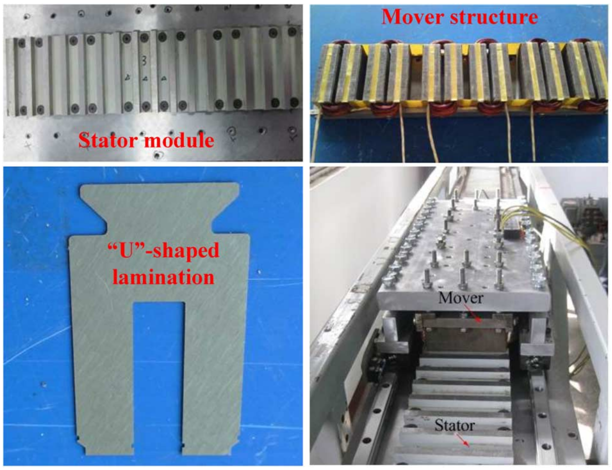

Fig. 5. The prototype of motor "AABBCC" with $\lambda_2 = (5 + 1/3)\tau_s$.

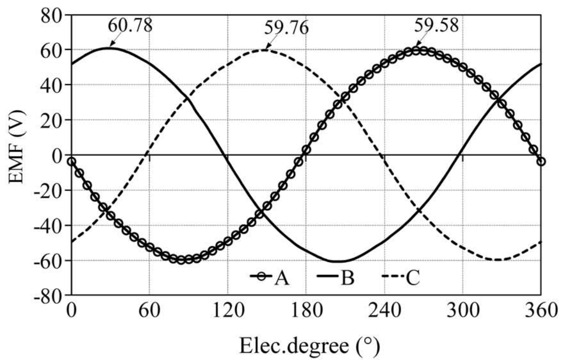

(a)

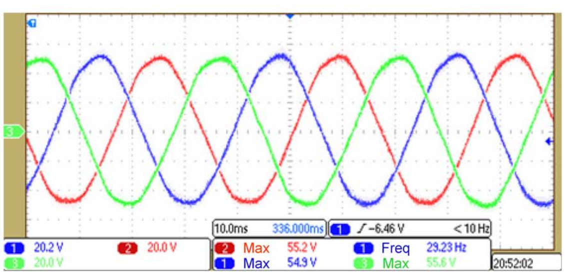

(b)

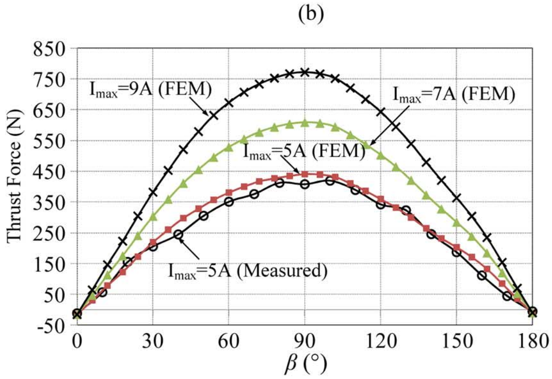

(c)

Fig. 6. Back-EMF waveforms at 1.05 m/s and Locked thrust force. (a) FEA results. (b) Experimental results. (c) Locked thrust force waveforms versus β at different currents.

exhibit a good agreement with the experimental ones. The discrepancies between the experimental and simulation results are about 10%, which we believe are mainly caused by the end-effects as in the stator-PM machines [23], [24], manufacturing imperfection and measurement error.

TABLE III
COEFFICIENTS λ_1 AND λ_2 OF DIFFERENT "ABCABC" MOTORS

τ_s/τ_m	λ_1	λ_2
12/10	$5\tau_s$	$5\tau_s/3$
12/11	$5.5\tau_s$	$11\tau_s/6$
12/12	$6\tau_s$	$2\tau_s$
12/13	$6.5\tau_s$	$13\tau_s/6$
12/14	$7\tau_s$	$7\tau_s/3$
12/15	$7.5\tau_s$	$2.5\tau_s$

III. CMLFSPM MOTORS WITH DIFFERENT τ_s/τ_m

In Section II, the structure and electromagnetic performances of different LFSPM motors with $\tau_s/\tau_m = 12/14$ have been investigated. It can be seen that the relative displacement between the two coils in each phase of the motor "ABCABC" and the stator are the same. Hence, it has asymmetrical back-EMF and bigger thrust force ripple. But for some MLFSPM motors with different τ_s/τ_m, coefficient λ_1 and λ_2 are different. Since λ_1 and λ_2 are two key coefficients of a MLFSPM motor, which not only affect the complementary characteristic but also define its phase number and armature winding connection, the structure and electromagnetic performances of the MLFSPM motors with different τ_s/τ_m, namely τ_s/τ_m = 12/10, 12/11, 12/12, 12/13, 12/15, are analyzed in this section. By using (1) and (2), coefficient λ_1 and λ_2 of "ABCABC" motors with different τ_s/τ_m can be calculated and listed in Table III.

It can be seen from Table III that the MLFSPM motor "ABCABC" with $\tau_s/\tau_m = 12/10$ is a three-phase motor because the relative displacement between phase A E-shaped modules and the adjacent phase E-shaped modules are mutually $\lambda_2 = (1 + 2/3)\tau_s$ apart, namely 240° apart. But this motor is not complementary because the relative displacement between the two coils of phase A and the stator are the same, namely having the same electrical degree. Hence, to obtain symmetrical back-EMF and smaller force ripple, the structures "ABC-ABC" and "AABBCC" need to be adopted in this MLFSPM motor with $\tau_s/\tau_m = 12/10$.

As aforementioned, the mover pole pitch τ_m is kept constant in this paper for all the LFSPM motors with different τ_s/τ_m. So, the mover length of motor "$4 * $ABC" with different τ_s/τ_m are the same and can be calculated as $L_m = 13\tau_m - 0.5w_{pm}$. The mover length of motor "ABC-ABC" with $\tau_s/\tau_m = 12/10$ can be calculated as $L_m = 12\tau_m - w_{pm} + 0.5\tau_s = 12.6\tau_m - w_{pm}$.

For the structure of "AABBCC" motors with $\tau_s/\tau_m = 12/10$, the minimum value of λ_1 can be calculated by using (7), (8), $\lambda_1 = 2.5\tau_s$. Also, the length of the three shortest mover length motors can be obtained by using (9)–(15):

$$L_m = \begin{cases} 75\tau_m/5 - w_{\mathrm{pm}}, & \lambda_2 = (4 + 1/6)\tau_s \\ 77\tau_m/5 - w_{\mathrm{pm}}, & \lambda_2 = (4 + 1/3)\tau_s\,. \\ 81\tau_m/5 - w_{\mathrm{pm}}, & \lambda_2 = (5 - 1/3)\tau_s \end{cases} \tag{16}$$

It can be seen from (16) that the maximum mover length of the above three motors at $w_{pm} = 0$ is about 115.4%, 1.5%, and

TABLE IV
CMLFSPM MOTORS WITH DIFFERENT τ_s/τ_m

Structure / τ_s/τ_m	ABCABC	ABC-ABC	2A2B2C	AABBCC			
				λ_2=(k+1/3) τ_s	λ_2=(k-1/3) τ_s	λ_2=(k+1/6) τ_s	λ_2=(k-1/6) τ_s
12/10		√					
12/11	√			√ (*k*=4)			
12/12			√		√ (*k*=5)		√ (*k*=5)
12/13	√				√ (*k*=5)	√ (*k*=5)	√ (*k*=5)
12/14		√		√ (*k*=5)		√ (*k*=5)	√ (*k*=5)
12/15				√ (*k*=5)	√ (*k*=6)	√ (*k*=5)	√ (*k*=6)

124.6% of the maximum mover length of motor "$4 * \mathrm{ABC}$", respectively. In this paper, if the maximum mover length of motor "AABBCC" is bigger than 110% of the maximum length of motor "$4 * \mathrm{ABC}$" then it will not be discussed. Hence, the structure "AABBCC" will not be adopted in MLFSPM motors with $\tau_s/\tau_m = 12/10$.

It can be seen from Table III that "ABCABC" motor with $\tau_s/\tau_m = 12/11$ and $\tau_s/\tau_m = 12/13$ are different from "ABCABC" motors with $\tau_s/\tau_m = 12/10$ and $\tau_s/\tau_m = 12/14$, which are three-phase motors with complementary characteristic because the relative position of the two coils of phase A are mutually 0° apart, namely $\lambda_1 = 5 + 0.5\tau_s$. Hence, the structure "ABC-ABC" is not suitable for these motors. But the "AABBCC" structures of these two motors also need to be analyzed in this section.

The mover length of motor "ABCABC" with $\tau_s/\tau_m = 12/11$ and $\tau_s/\tau_m = 12/13$ are the same and can be calculated as $L_m = 12\tau_m - w_{pm}$.

For motor "AABBCC" with $\tau_s/\tau_m = 12/11$, the minimum value of λ_1 can be calculated using (3), (7), (8), $\lambda_1 = 2.5\tau_s$. Also, the length of the shortest mover length motor can be obtained by using (9)–(15):

$$L_m = 156\tau_m/11 - w_{pm}, \quad \lambda_2 = (4 + 1/3)\tau_s. \tag{17}$$

So, the maximum mover length of the motor at $w_{pm} = 0$ can be calculated by (17), which is about 109.1% of the maximum length of motor "$4 * \mathrm{ABC}$", respectively.

For motor "AABBCC" with $\tau_s/\tau_m = 12/13$, the minimum value of λ_1 also can be calculated using (3), (7), (8), $\lambda_1 = 2.5\tau_s$. Also, the length of the three shortest mover length motors can be obtained using (9)–(15):

$$L_m = \begin{cases} 168\tau_m/13 - w_{pm}, & \lambda_2 = (5 - 1/3)\tau_s \\ 172\tau_m/13 - w_{pm}, & \lambda_2 = (5 - 1/6)\tau_s \\ 0\tau_m/13 - w_{pm}, & \lambda_2 = (5 + 1/6)\tau_s \end{cases}. \quad ()$$

The maximum mover length of above three motors at $w_{pm} = 0$ can be calculated by (), which is about 99.4%, 101.8%, and 106.5% of the maximum length of motor "$4 * \mathrm{ABC}$", respectively.

It can be seen from Table III that "ABCABC" and "$4 * \mathrm{ABC}$" motors with $\tau_s/\tau_m = 12/12$ are single-phase motors. The relative displacement between all adjacent E-shaped modules and the stator is the same. Hence, in order to obtain three phase motors, two methods can be adopted.

First, the "AABBCC" structure is adopted. The minimum value of λ_1 can be calculated using (3), (7), (8), $\lambda_1 = 2.5\tau_s$. Also, the length of the two shortest mover length motors can be obtained by using (9)–(15):

$$L_m = \begin{cases} 41.5\tau_m/3 - w_{pm}, & \lambda_2 = (5 - 1/3)\tau_s \\ 42.5\tau_m/3 - w_{pm}, & \lambda_2 = (5 - 1/6)\tau_s \end{cases}. \tag{19}$$

So, the maximum mover length of the above two motors at $w_{pm} = 0$ can be calculated by (19), which is about 106.4% and 109% of the maximum length of motor "$4 * \mathrm{ABC}$", respectively.

Second, it should be noted that due to the symmetrical E-shaped structure with $\tau_s/\tau_m = 12/12$, even though $\lambda_1 = j\tau_s$ $(j = 2)$, the negative and positive back-EMF waveforms induced in coil A1, coil A2, and phase coil A are symmetrical. Hence, $\lambda_1 = 2\tau_s$ and λ_2 satisfying (4) can be adopted in this motor, which is named as motor "2A2B2C".

So, the length of the four shortest mover "2A2B2C" motors can be obtained by (9)–(15):

$$L_m = \begin{cases} 37\tau_m/3 - w_{pm}, & \lambda_2 = (4 + 1/6)\tau_s \\ 38\tau_m/3 - w_{pm}, & \lambda_2 = (4 + 1/3)\tau_s \\ 40\tau_m/3 - w_{pm}, & \lambda_2 = (5 - 1/3)\tau_s \\ 41\tau_m/3 - w_{pm}, & \lambda_2 = (5 - 1/6)\tau_s \end{cases}. \tag{20}$$

The maximum mover length of above four motors at $w_{pm} = 0$ can be calculated by (20), which is about 94.9%, 97.4%, 102.6%, and 105.1% of the maximum length of motor "$4 * \mathrm{ABC}$", respectively.

It can be seen from Table III that "ABCABC" motor with $\tau_s/\tau_m = 12/15$ is a four-phase or two-phase motor and motor "$4 * \mathrm{ABC}$" with $\tau_s/\tau_m = 12/15$ is a two-phase or single-phase motor. Hence, to obtain a three-phase motor with $\tau_s/\tau_m = 12/15$, the "AABBCC" structure need to be adopted. The minimum value of λ_1 can be calculated using (3), (7), (8), $\lambda_1 = 2.5\tau_s$. Also, the length of the four shortest mover length motors can be obtained by (9)–(15):

$$L_m = \begin{cases} 4\tau_m/15 - w_{pm}, & \lambda_2 = (5 + 1/6)\tau_s \\ 192\tau_m/15 - w_{pm}, & \lambda_2 = (5 + 1/3)\tau_s \\ 196\tau_m/15 - w_{pm}, & \lambda_2 = (6 - 1/3)\tau_s \\ 40\tau_m/3 - w_{pm}, & \lambda_2 = (6 - 1/6)\tau_s \end{cases}. \tag{21}$$

So, the maximum mover length of the above four motors at $w_{pm} = 0$ can be calculated by (21), which is about 94.4%, 98.5%, 100.5%, and 102.56% of the maximum length of motor "$4 * \mathrm{ABC}$", respectively.

It should be mentioned that some "ABC-ABC" motors with $\tau_s/\tau_m = 12/10$, 12/11, 12/12, 12/13, 12/14, and 12/15 also can be obtained directly using (3), (4), but not be listed in this paper.

TABLE V
COMPARISON OF CMLFSPM MOTORS WITH $\tau_s/\tau_m = 12/10, 12/11$

τ_s/τ_m	12/10	12/11	
Structure	ABC-ABC λ_2=(1+2/3)τ_s	**ABCABC** λ_2=(2-1/6)τ_s	AABBCC, λ_2=(4+1/3)τ_s
k_{st}	1.9	**1.9**	1.9
k_{sty}	2	**2**	2
EMF (V)	51.97	**62.9**	62.2
$F_{\_avg}$ (N)	608	**714.7**	707.77
$F_{\_cog}$ (N)	98.8	**47.08**	44.72
$F_{\_ripple}$ (N)	92.3	**104.1**	95.9
V_{m_iron} (cm^3)	1958.04	**1958.04**	1958.04
V_{PM} (cm^3)	Same	**Same**	Same
M_{copper} (kg)	Same	**Same**	Same
L_m (mm)	87τ_m/7-w_{pm}	**84τ_m/7-w_{pm}**	156τ_m/11-w_{pm}
L_m/L_{m1}(%)	95%	**91.6%**	108.5%

Up to now, the structures of some CMLFSPM motors with different τ_s/τ_m have been investigated. The detailed structures are listed in Table IV for the next step work.

IV. Electromagnetic Performance Comparison

A. CMLFSPM Motors With τ_s/τ_m = 12/10 and 12/11

Based on FEA results, for motor "ABC-ABC" with $\tau_s/\tau_m = 12/10$, F_cog and F_ripple reach the minimum value at $k_{st} = 1.9$ and F_avg is about 99.98% of the maximum value at $k_{st} = 1.8$. Hence, $k_{st} = 1.9$ is adopted in this motor. Similarly, $k_{st} = 1.9$ is also adopted in motor "ABCABC" and motor "AABBCC" with $\lambda_2 = (4+1/3)\tau_s$. For comparison, the detailed electromagnetic performance and dimensions are listed in Table V. It can be seen that F_avg, F_cog, F_ripple, and mover length of motor "ABCABC" is 101%, 105.3%, 108.6%, and 84% of motor "AABBCC" with $\lambda_2 = (4+1/3)\tau_s$, respectively. Hence, motor "ABCABC" is chosen to be the best structure with $\tau_s/\tau_m = 12/11$ for comparison with other motors.

B. CMLFSPM Motors With $\tau_s/\tau_m = 12/12$

For motor "AABBCC" with $\lambda_2 = (5-1/3)\tau_s$, F_cog reaches the minimum value at $k_{st} = 1.9$, its F_avg is about 96% of the maximum value at $k_{st} = 1.5$. While F_ripple reaches the minimum value at $k_{st} = 1.2$, its F_avg is about 98.32% of the maximum value at $k_{st} = 1.5$. Also, F_ripple and F_cog at $k_{st} = 1.9$ are about 43.8% and 127.6% of the ones at $k_{st} = 1.2$, respectively. Hence, $k_{st} = 1.2$ is adopted in this motor. Similarly, $k_{st} = 1.2$ is also adopted in motor "AABBCC" with $\lambda_2 = (5-1/6)\tau_s$. The detailed electromagnetic performances and dimensions are listed in Table VI.

F_cog and F_ripple of motors "2A2B2C" with $\lambda_2 = (4+1/6)\tau_s$ and $\lambda_2 = (5-1/6)\tau_s$ are all reach their minimum value at $k_{st} = 1.9$, while their F_avg is about 95.8% and 95.84% of its maximum value at $k_{st} = 1.5$, respectively. Hence, $k_{st} = 1.9$ is adopted in these two motors. Similarly, $k_{st} = 1.2$ is adopted in these two motors. The detailed electromagnetic performance and dimensions of these four motors are listed in Table VII. It can be seen from Tables VI and VII that, by considering the mover length, F_avg, F_ripple, and F_cog, motor "2A2B2C" with $\lambda_2 = (4+1/3)\tau_s$ is chosen to be the best structure with $\tau_s/\tau_m = 12/12$ for comparison with other motors.

TABLE VI
COMPARISON OF BOTH "AABBCC" MOTORS WITH $\tau_s/\tau_m = 12/12$

Structure	**AABBCC**	
	λ_2=(5-1/3)τ_s	λ_2=(5-1/6)τ_s
k_{st}	1.2	1.2
k_{sty}	2	2
EMF (V)	66	66.4
$F_{\_avg}$ (N)	**767.6**	765.6
$F_{\_cog}$ (N)	**52.9**	46.4
$F_{\_ripple}$ (N)	**133.1**	120.5
V_{m_iron} (cm^3)	1958.04	1958.04
V_{PM} (cm^3)	Same	Same
M_{copper} (kg)	Same	Same
L_m (mm)	41.5τ_m/3-w_{pm}	42.5τ_m/3-w_{pm}
L_m/L_{m1} (%)	**107.1%**	109.7%

TABLE VII
COMPARISON OF THE FOUR "2A2B2C" MOTORS WITH $\tau_s/\tau_m = 12/12$

Structure	2A2B2C			
	λ_2=(4+1/6)τ_s	**λ_2=(4+1/3)τ_s**	λ_2=(5-1/3)τ_s	λ_2=(5-1/6)τ_s
k_{st}	1.9	**1.2**	1.2	1.9
k_{sty}	2	**2**	2	2
EMF (V)	66.97	**67.56**	66.68	66.78
$F_{\_avg}$ (N)	754.51	**772.54**	768.9	748.37
$F_{\_cog}$ (N)	45.08	**57.43**	47.32	48.8
$F_{\_ripple}$ (N)	181.73	**119.6**	129.2	183
V_{m_iron} (cm^3)	1958.04	**1958.04**	1958.04	1958.04
V_{PM} (cm^3)	Same	**Same**	Same	Same
M_{copper} (kg)	Same	**Same**	Same	Same
L_m (mm)	37τ_m/3-w_{pm}	**38τ_m/3-w_{pm}**	40τ_m/3-w_{pm}	41τ_m/3-w_{pm}
L_m/L_{m1} (%)	95.48%	**98%**	103.2%	105.8%

C. CMLFSPM Motors With $\tau_s/\tau_m = 12/13$

For the four CMLFSPM motors with $\tau_s/\tau_m = 12/13$, their F_avg all reach the maximum value and their F_ripple is near to the minimum value at $k_{st} = 1.3$. However, at this point their cogging force is too bigger. Hence, $k_{st} = 1.6$ is chosen to be the optimal point for motor "ABCABC". Similarly, $k_{st} = 1.5$ is chosen to be the optimal point for motors "AABBCC" with $\lambda_2 = (5-1/3)\tau_s$, $\lambda_2 = (5-1/6)\tau_s$, and $\lambda_2 = (5+1/6)\tau_s$. The detailed electromagnetic performances and dimensions of the four CMLFSPM motors are listed in Table VIII. It can be seen that F_avg of the four motors is nearly the same, motor "ABCABC" has the shortest mover, and motor "AABBCC" with $\lambda_2 = (5-1/6)\tau_s$ has the smallest cogging force and relative smaller F_ripple. Hence, motor "ABCABC" and "AABBCC" with $\lambda_2 = (5-1/6)\tau_s$ are chosen to be the two best structures when $\tau_s/\tau_m = 12/11$ for comparison with other motors.

D. CMLFSPM Motors With $\tau_s/\tau_m = 12/15$

F_cog and F_ripple of motor "AABBCC" with $\lambda_2 = (4+1/6)\tau_s$, $\lambda_2 = (4+1/3)\tau_s$, and $\lambda_2 = (5-1/3)\tau_s$ reach the minimum value at $k_{st} = 1.7$. However, at this point their F_avg is only about 88.3%, 87.7%, and 88.39% of their maximum value at $k_{st} = 1.2$, respectively. Also, the maximum F_avg of motor

TABLE VIII
COMPARISON OF THE FOUR CMLFSPM MOTORS WITH $\tau_s/\tau_m = 12/13$

Structure	**ABCABC**	AABBCC		
		λ_2=(5-1/3)τ_s	**λ_2=(5-1/6)τ_s**	λ_2=(5+1/6)τ_s
k_{st}	**1.6**	1.5	**1.5**	1.5
k_{sty}	**2**	2	**2**	2
EMF (V)	**67.29**	66.95	**67.06**	66.4
$F_{\_avg}$ (N)	**770.9**	774.9	**771.67**	771.1
$F_{\_cog}$ (N)	**26.3**	**37.1**	**18.17**	**23.2**
$F_{\_ripple}$ (N)	**89**	79.9	**52.4**	43.17
V_{m_iron} (cm^3)	**1958.04**	1958.04	**1958.04**	1958.04
V_{PM} (cm^3)	**Same**	Same	**Same**	Same
M_{copper} (kg)	**Same**	Same	**Same**	Same
L_m (mm)	**$12\tau_m$-w_{pm}**	$168\tau_m$/13-w_{pm}	**$172\tau_m$/13-w_{pm}**	$180\tau_m$/13-w_{pm}
L_m/ L_{m1} (%)	**91.6%**	98.8%	**101.1%**	105.9%

TABLE IX
COMPARISON OF THE OPTIMAL CMLFSPM MOTORS WITH DIFFERENT τ_s/τ_m

τ_s/τ_m	12/10	12/11	12/12	**12/13**		12/14	12/15
Structure	ABC-ABC	ABCABC	2A2B2C	**ABCABC**	**AABBCC**	AABBCC	AABBCC
λ_2	λ_2=(1+2/3)τ_s	λ_2=(2-1/6)τ_s	λ_2=(4+1/3)τ_s	**λ_2=(2+1/6)τ_s**	**λ_2=(5-1/6)τ_s**	λ_2=(4+1/3)τ_s	λ_2=(5+1/3)τ_s
k_{st}	1.9	1.9	1.2	**1.6**	**1.5**	1.1	1.2
k_{sty}	2	2	2	**2**	**2**	1.5	1.5
v (m/s)	1.5	1.5	1.5	**1.5**	**1.5**	1.5	1.5
EMF (V)	51.97	62.9	67.56	**67.29**	**67.06**	61.3	52.7
F_avg (N)	608	714.7	**772.54**	**770.9**	**771.67**	711.86	600
F_cog (N)	98.8	47.08	57.43	**26.3**	**18.17**	**27.89**	41.33
F_ripple (N)	92.3	104.1	119.6	**89**	**52.4**	48	56.75
P_o (W)	912	1071	1158.81	**1156.35**	**1157.51**	1067.79	900
V_m (cm^3)	1958.04	1958.04	1958.04	**1958.04**	**1958.04**	1958.04	1958.04
V_{pm} (cm^3)	Same	Same	Same	**Same**	**Same**	Same	Same
M_{cu} (kg)	Same	Same	Same	**Same**	**Same**	Same	Same
P_{cu} (W)	162	162	162	**162**	**162**	162	162
P_{core} (W)	6.8	7.6	7.4	**8.3**	**7.3**	7.4	7.3
η (%)	83.4%	86.3%	87.24%	**87.16%**	**87.24%**	86.3%	84.2%
L_m (mm)	$87\tau_m$/7-w_{pm}	$84\tau_m$/7-w_{pm}	$38\tau_m$/3-w_{pm}	**$12\tau_m$-w_{pm}**	**$172\tau_m$/13-w_{pm}**	$93\tau_m$/7-w_{pm}	$192\tau_m$/15-w_{pm}
L_m/L_{m1} (%)	95%	91.6%	98%	**91.6%**	**101.1%**	101.6%	97.8%

"AABBCC" with $\lambda_2 = (4 + 1/3)\tau_s$ at $k_{st} = 1.2$ is the biggest one and its F_cog, F_ripple are smaller than the one of other motors. Hence, motor "AABBCC" with $\lambda_2 = (4 + 1/3)\tau_s$ and $k_{st} = 1.2$ is chosen to be the best structure when $\tau_s/\tau_m = 12/15$ for comparison with other motors.

E. Comparison of the Optimal CMLFSPM Motor

For comparison, the detailed electromagnetic performances and dimensions of the optimal CMLFSPM motors with different τ_s/τ_m are listed in Table IX.

From Table IX, the electromagnetic performance of the seven optimal motors can be summarized as follows.

- F_avg and EMF of motor "ABCABC" and "AABBCC" with $\tau_s/\tau_m = 12/13$ are nearly the same as the one of the biggest one of motor "2A2B2C" with $\tau_s/\tau_m = 12/12$.
- Motor "AABBCC" with $\tau_s/\tau_m = 12/13$ can offer the smallest F_cog, the second-smallest F_ripple and its mover length is about 103.2% of motor "2A2B2C".
- F_cog, F_ripple, and mover length of motor "AABBCC" with $\tau_s/\tau_m = 12/13$ are about 71.1%, 58.9%, and 110.4% of motor "ABCABC" with $\tau_s/\tau_m = 12/13$, respectively.

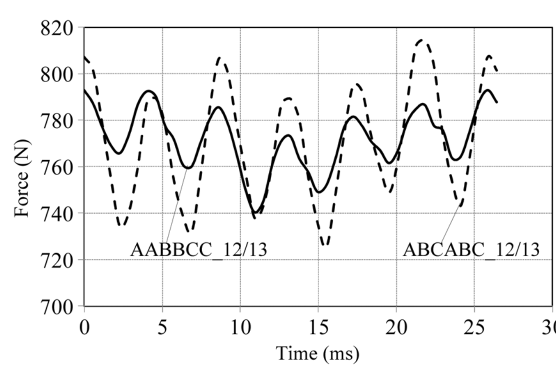

Fig. 7. The transient thrust forces waveforms of both motors with $\tau_s/\tau_m = 12/13$ as listed in Table IX.

- Hence, considering the electromagnetic performance, motor "ABCABC" and "AABBCC" with $\tau_s/\tau_m = 12/13$ are the two best motors.
- Their F_avg (771 N) is about 126.8%, 107.9%, 99.8%, 108.3%, and 128.5% of the CMLFSPM motors with $\tau_s/\tau_m =$ 12/10, 12/11, 12/12, 12/14, 12/15, respectively.

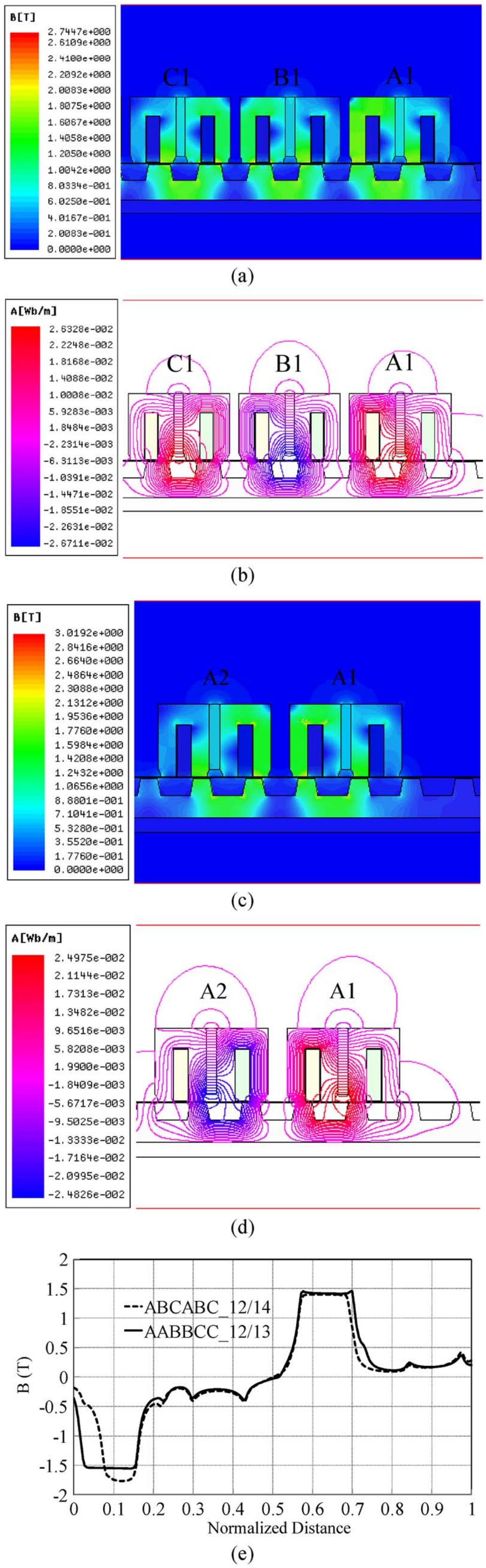

Fig. 8. Partial open circuit magnetic flux density and flux lines distribution of the two optical CMLFSPM motors. (a) Flux density of motor "ABCABC" with $\tau_s/\tau_m = 12/13$. (b) Flux line of motor "ABCABC" with $\tau_s/\tau_m = 12/13$. (c) Flux density of motor "AABBCC" with $\tau_s/\tau_m = 12/14$. (d) Flux line of motor "AABBCC" with $\tau_s/\tau_m = 12/14$. (e) Air-gap flux density under the "E"-shaped coil-A1 of both motors.

The waveforms of the transient thrust forces of both motors with $\tau_s/\tau_m = 12/13$ at the rated speed and phase current are shown in Fig. 7.

- It should be mentioned that the teeth volume of the two best motors is bigger than motor "2A2B2C" with $\tau_s/\tau_m = 12/10$, motor "AABBCC" with $\tau_s/\tau_m = 12/14$, and motor "AABBCC" with $\tau_{\mathrm{s}}/\tau_{\mathrm{m}} = 12/15$ due to their bigger k_{st}.
- The core loss of the six CMLFSPM motors can be calculated by using the method discussed in [25]. Also, the copper loss can be calculated by the applied current and phase resistance. By neglecting the friction loss, the efficiency of the six CMLFSPM motors at the rated current and speed can be calculated and listed in Table IX. It can be seen that the three motors with $\tau_s/\tau_m = 12/12$ and 12/13 can offer higher efficiency which is about 87.2%. It should be mentioned that the armature winding filling ratio (0.4) is designed relatively small in this paper. Hence, the efficiency of the six motors can be increased by using bigger diameter wire.
- It can be seen from Fig. 8(a)–(d) that the flux density in the mover teeth, yoke and stator yoke of the two motors is about in the range of 1.5 T to 1.8 T. However, the flux density in the partial mover teeth-tip of both motors is nearly 2.0 T. Also, for the two motors, there are some flux leakages at the mover end, mover top, and adjacent stator teeth in the inner part of the E-shaped module. Fig. 8(e) shows the flux density waveforms of both motors in the air gap under the "E"-shaped coil-A1 when the flux linkage in phase A reaches the maximum value. It can be seen that the positive peak value of the air gap density of both motors are nearly the same, while the negative peak value of motor "AABBCC" with $\tau_{\mathrm{s}}/\tau_{\mathrm{m}} = 12/14$ is bigger than the one of motor "ABCABC" with $\tau_{\mathrm{s}}/\tau_{\mathrm{m}} = 12/13$. However, both the positive and negative flat portion of the air gap flux density of motor "ABCABC" with $\tau_{\mathrm{s}}/\tau_{\mathrm{m}} = 12/13$ are wider than that of motor "AABBCC" with $\tau_{\mathrm{s}}/\tau_{\mathrm{m}} = 12/14$. Hence, motor "ABCABC" with $\tau_{\mathrm{s}}/\tau_{\mathrm{m}} = 12/13$ can offer higher back-EMF and thrust force than motor "AABBCC" with $\tau_{\mathrm{s}}/\tau_{\mathrm{m}} = 12/14$ by using the same volume of PM, mover iron, and armature winding.

V. Conclusion

In this paper, the structure, dimensions, operation principle, and electromagnetic performance of a conventional LFSPM motor and three structures of MLFSPM motors with $\tau_s/\tau_m = 12/14$ have been optimized and compared by means of FEA. To verify the simulation results of these LFSPM motors, a prototype motor has been built and tested. The experimental results agree well with the predicted results from FEA. Then, the structure and electromagnetic performance of some CMLFSPM motors with different τ_s/τ_m, namely τ_s/τ_m = 12/10, 12/11, 12/12, 12/13, and 12/15 have been optimized and compared using FEA. Based on the electromagnetic performance and dimension of the optimal CMLFSPM motors with different τ_s/τ_m, the CMLFSPM motors with $\tau_s/\tau_m = 12/13$ are chosen to be the two best motors. The research results are very helpful to select and design this kind of complementary and modular LFSPM motors.

ACKNOWLEDGMENT

This work was supported in part by the "973" Program of China under Project 2013CB035603, the National Natural Science Foundation of China under Project 50907031, the Specialized Research Fund for the Doctoral Program of Higher Education of China under Project 20090092110034, the Scientific Research Foundation of Graduate School of Southeast University, and the Program for Postgraduate Research Innovation in General Universities of Jiangsu Province 2010 under Project X10B_066Z.

REFERENCES

[1] J. F. Gieras and Z. J. Piech, *Linear Synchronous Motors: Transportation and Automation Systems*. Boca Raton, FL: CRC Press, 2000.

[2] A. Boldea and S. Nasar, *Linear Motion Electromagnetic Devices*. New York: Taylor & Francis, 2001.

[3] T. Higuchi and S. Nonaka, "On the design of high efficiency linear induction motors for linear metro," *Elect. Eng. Jpn.*, vol. 137, no. 2, pp. 36–43, Aug. 2001.

[4] S. Yoon, J. Hur, and D. Hyun, "A method of optimal design of single-sided linear induction motor for transit," *IEEE Trans. Magn.*, vol. 33, no. 5, pp. 4215–4217, Sep. 1997.

[5] S. Nonaka and T. Higuchi, "Design of single-sided linear induction motors for urban transit," *IEEE Trans. Veh. Technol.*, vol. 37, no. 3, pp. 167–173, Aug. 1988.

[6] R. Cao, M. Cheng, C. Mi, W. Hua, and W. Zhao, "A linear doubly salient permanent magnet motor with modular and complementary structure," *IEEE Trans. Magn.*, vol. 47, no. 12, pp. 4809–4821, Dec. 2011.

[7] S.-U. Chung, D.-H. Kang, J.-H. Chang, J.-W. Kim, and J.-Y. Lee, "New configuration of flux reversal linear synchronous motor," in *Proc. ICEMS2007*, Seoul, Korea, Oct. 2007, pp. 864–867.

[8] S.-U. Chung, H.-J. Lee, and S.-M. Hwang, "A novel design of linear synchronous motor using FRM topology," *IEEE Trans. Magn.*, vol. 44, no. 6, pp. 1514–1517, Jun. 2008.

[9] Z. Q. Zhu, X. Chen, and J. Chen, "Novel linear flux switching permanent magnet machines," in *Proc. ICEMS2008*, 2008, pp. 2948–2953.

[10] M. Cheng, W. Hua, J. Zhang, and W. Zhao, "Overview of stator permanent magnet brushless machines," *IEEE Trans. Ind. Electron.*, vol. 85, no. 11, pp. 5087–5101, 2011.

[11] Y. Liao, F. Liang, and T. A. Lipo, "A novel permanent magnet machine with doubly salient structure," in *Proc. IEEE IAS Annu. Conf.*, 1992, pp. 308–314.

[12] R. P. Deodhar, S. Andersson, I. Boldea, and T. J. E. Miller, "The flux-reversal machine: A new blushless doubly-salient permanent-magnet machine," in *Proc. IEEE IAS Annu. Conf.*, 1996, pp. 786–793.

[13] E. Hoang, A. H. Ben-Ahmed, and J. Lucidarme, "Switching flux permanent magnet polyphased machines," in *Proc. Eur. Conf. Power Electron. Appl.*, 1997, pp. 903–908.

[14] J. Zhang, M. Cheng, Z. Chen, and W. Hua, "Comparison of stator-mounted permanent-magnet machines based on a general power equation," *IEEE Trans. Energy Convers.*, vol. 24, no. 4, pp. 826–834, Dec. 2009.

[15] Z. Q. Zhu and J. T. Chen, "Advanced flux-switching permanent magnet brushless machines," *IEEE Trans. Magn.*, vol. 46, no. 6, pp. 1447–1453, Jun. 2010.

[16] T. Raminosoa, C. Gerada, and M. Galea, "Design considerations for a fault-tolerant flux-switching permanent-magnet machine," *IEEE Trans. Ind. Electron.*, vol. 58, no. 7, pp. 28–2825, Jul. 2011.

[17] W. Zhao, M. Cheng, W. Hua, H. Jia, and R. Cao, "Back-EMF harmonic analysis and fault-tolerant control of flux-switching permanent-magnet machine with redundancy," *IEEE Trans. Ind. Electron.*, vol. 58, no. 5, pp. 1926–1935, May 2011.

[18] C. Wang, J. Shen, and Y. Wang, "A new method for reduction of detent force in permanent magnet flux-switching linear motors," *IEEE Trans. Magn.*, vol. 45, no. 6, pp. 2843–2846, Jun. 2009.

[19] M. Jin, C. Wang, and J. Shen, "A modular permanent magnet flux-switching linear machine with fault tolerant capability," *IEEE Trans. Magn.*, vol. 45, no. 8, pp. 3179–36, Aug. 2009.

[20] R. Cao, M. Cheng, C. Mi, W. Hua, X. Wang, and W. Zhao, "Modeling of a complementary and modular linear flux-switching permanent magnet motor for urban rail transit applications," *IEEE Trans. Energy Convers.*, vol. 27, no. 2, pp. 489–497, Jun. 2012.

[21] A. Chen, N. Rotevatn, R. Nilssen, and A. Nysveen, "Characteristic investigations of a new three-phase flux-switching permanent magnet machine by FEM simulations and experimental verification," in *Proc. ICEMS2009*, Tokyo, Japan, Nov. 2009, pp. 1–6.

[22] J. T. Chen and Z. Q. Zhu, "Comparison of all- and alternate-poles-wound flux-switching PM machines having different stator and rotor pole numbers," *IEEE Trans. Ind. Appl.*, vol. 46, no. 4, pp. 1406–1415, Jul./Aug. 2010.

[23] Z. Q. Zhu, Y. Pang, W. Hua, M. Cheng, and D. Howe, "Investigation of end effect in permanent magnet brushless machines having magnets on the stator," *J. Appl. Phys.*, vol. 99, no. 8, pp. 1–3, Apr. 2006, 08R319.

[24] W. Hua and M. Cheng, "Static characteristic of doubly-salient brushless machines having magnets in the stator considering end-effect," *Elect. Mach. Power. Syst.*, vol. 36, no. 7, pp. 754–770, Jul. 2008.

[25] R. Cao, C. Mi, and M. Cheng, "Quantitative comparison of flux-switching permanent magnet motors with interior permanent magnet motor for EV, HEV, and PHEV applications," *IEEE Trans. Magn.*, vol. 48, no. 8, pp. 2374–2384, Aug. 2012.

Ruiwu Cao (S'10) received the B.S. degree from Yancheng Institute of Technology, Yancheng, China, in 2004, and the M.S. degree from Southeast University, Nanjing, China, in 2007. He has been working toward the Ph.D. degree in school of Southeast University, Nanjing, China, since 2009, all in electrical engineering.

From 2007 to 2009, He was a Hardware Electrical Engineer with Electronic Drive System R&D center of BSH electrical Appliances (Jiangsu) Co., Ltd. From August 2010 to November 2011, he was a joint Ph.D. student founded by China Scholarship Council with the College of Electrical and Computer Science, University of Michigan, Dearborn, where he worked on permanent magnet motors for EV, HEV and PHEV application. His areas of interests include design, analysis, and control of permanent-magnet machines.

Ming Cheng (M'01–SM'02) received the B.Sc. and M.Sc. degrees from the Department of Electrical Engineering, Southeast University, China, in 1982 and 1987, respectively, and Ph.D. degree from the Department of Electrical and Electronic Engineering, The University of Hong Kong, Hong Kong, in 2001.

Since 1987, he has been with Southeast University, where he is currently a Professor in the School of Electrical Engineering and the Director of the Research Center for Wind Power Generation. As a Visiting Professor, he worked in WEMPEC, The University of Wisconsin-Madison, USA from January to April, 2011, and in the Department of Energy Technology, Aalborg University, Denmark from June to July, 2012, respectively. His teaching and research interests include electrical machines, motor drives for electric vehicles and renewable energy generation. He has authored or coauthored over 250 technical papers and 4 books, and holds 50 patents in these areas. He is the recipient of "IET Premium Award in Electric Power Application", "GM Automotive Innovative Talent Award for China University" and "SAE Environmental Excellence in Transportation (E2T) Award".

Prof. Cheng is a Fellow of The Institution of Engineering and Technology. He has served as chair and organizing committee member for many international conferences.

Chris Mi (S'00–A'01–M'01–SM'03–F'12) received the B.S. and M.S. degrees from Northwestern Polytechnical University, Xi'an, China, and the Ph.D. degree from the University of Toronto, Toronto, ON, Canada, all in electrical engineering.

He is a Professor with the University of Michigan, Dearborn, and the Director of the newly established DOE GATE Center for Electric Drive Transportation. Previously, he was an Electrical Engineer with General Electric Canada Inc. His research interests include electric drives, power electronics, electric machines; renewable energy systems; electrical and hybrid vehicles. He has conducted extensive research and published more than 100 articles.

Dr. Mi is the recipient of "Distinguished Teaching Award" and "Distinguished Research Award" of University of Michigan-Dearborn. He is also a recipient of the 2007 IEEE Region 4 "Outstanding Engineer Award," "IEEE Southeastern Michigan Section Outstanding Professional Award." and the "SAE Environmental Excellence in Transportation (E2T) Award." He was the Chair (2008–2009) and Vice Chair (2006–2007) of the IEEE Southeastern Michigan Section. He was the general Chair of the 5th IEEE Vehicle Power and Propulsion Conference held in Dearborn, Michigan, USA in September 6–11, 2009. He is Associate Editor of IEEE Transactions on Vehicular Technology and IEEE Transactions on Power Electronics-Letters, Senior Editor, *IEEE Vehicular Technology Magazine*, Guest Editor, *International Journal of Power Electronics*, Editorial Board, *International Journal of Electric and Hybrid Vehicles*, Editorial Board, *IET Electrical Systems in Transportation*, Associate Editor of *Journal of Circuits, Systems, and Computers* (2007–2009), and Associate Editor for IEEE Transactions on Industry Applications.

Wei Hua (M'07) was born in Jiangsu, China, in 1978. He received the B.S. and Ph.D. degrees in electrical engineering from Southeast University, Nanjing, China, in 2001 and 2007, respectively.

He is currently with Southeast University, where he is a Professor and Deputy Dean of School of Electrical Engineering. His areas of interest include design, analysis, and control of the novel permanent magnet machines and switched reluctance machines. He has authored more than 100 published papers on those topics.

Wenxiang Zhao (M'08) was born in Jilin, China, in 1976. He received the B.S. and M.S. degrees in electrical engineering from Jiangsu University, Zhenjiang, China, in 1999 and 2003, respectively, and the Ph.D. degree in electrical engineering at Southeast University, Nanjing, China, in 2010.

Since 2003, he has been with Jiangsu University, where he is currently an Associate Professor in the School of Electrical Information Engineering. His areas of interest include electric machine design, modeling, fault analysis and intelligent control.